AMERICAN SOCIETY FOR MICROBIOLOGY | Journal of Bacteriology®

RESEARCH ARTICLE

R-Type Fonticins Produced by *Pragia fontium* Form Large Pores with High Conductance

Klára Látrová,[a] Tereza Dolejšová,[a] Lucia Motlová,[a,c] Gabriela Mikušová,[a] Juraj Bosák,[b] Kateřina Snopková,[b] David Šmajs,[b] Ivo Konopásek,[a] Radovan Fišer[a]

[a]Department of Genetics and Microbiology, Faculty of Science, Charles University, Prague, Czech Republic
[b]Department of Biology, Faculty of Medicine, Masaryk University, Kamenice, Brno, Czech Republic
[c]Imaging Methods Core Facility at Biocev, Faculty of Science, Charles University, Vestec, Czech republic

ABSTRACT Fonticins are phage tail-like bacteriocins produced by the Gram-negative bacterium *Pragia fontium* from the family *Budviciaceae*. This bacterium produces contractile-type particles that adsorb on the surface of sensitive bacteria and penetrate the cell wall, probably during contraction, in a way similar to the type VI secretion system. We characterized the pore-forming activity of fonticins using both living cells and *in vitro* model membranes. Using a potassium leakage assay, we show that fonticins are able to permeabilize sensitive cells. On black lipid membranes, single-pore conductance is about 0.78 nS in 1 M NaCl and appears to be linearly dependent on the increasing molar strength of NaCl solution, which is a property of considerably large pores. In agreement with these findings, fonticins are not ion selective for Na^+, K^+, and Cl^-. Polyethylene glycol 3350 (PEG 3350) molecules of about 3.5 nm in diameter can enter the fonticin pore lumen, whereas the larger molecules cannot pass the pore. The size of fonticin pores was confirmed by transmission electron microscopy. The terminal membrane-piercing complex of the fonticin tube probably creates a selective barrier restricting passage of macromolecules.

IMPORTANCE Phage tail-like bacteriocins are now the subject of research as potent antibacterial agents due to their narrow host specificity and single-hit mode of action. In this work, we focused on the structure and mode of action of fonticins. According to some theories, related particles were initially adapted for passage of double-stranded DNA (dsDNA) molecules, but fonticins changed their function during the evolution; they are able to form large pores through the bacterial envelope of Gram-negative bacteria. As various pore-forming proteins are extensively used for nanopore sequencing and stochastic sensing, we decided to investigate the pore-forming properties of fonticin protein complexes on artificial lipid membranes. Our research revealed remarkable structural properties of these particles that may have a potential application as a nanodevice.

KEYWORDS fonticin, phage tail-like bacteriocins, black lipid membranes, membrane pore formation, conductance, electric current, electron microscopy, single-pore conductance

Phage tail-like bacteriocins (PTLBs) are high-molecular-weight protein complexes produced by a wide spectrum of eubacteria. These nanoscale-size particles are closely related to contractile tail bacteriophages (1), the type VI secretion system (2), *Photorhabdus* virulence cassettes (3), and some other contractile ejection systems, sharing the function and mechanism of penetrating the bacterial envelope (4, 5); therefore, PTLBs play an important role in bacterial interactions.

PTLBs occur in two morphologically different forms, contractile rigid particles (R-type) and noncontractile but flexible particles (F-type). R-type particles have evolutional relations with P2 phages from the family *Myoviridae*. On the other hand, F-type particles are derived

Editor Mohamed Y. El-Naggar, University of Southern California

Address correspondence to Radovan Fišer, fiserr@natur.cuni.cz.

The authors declare no conflict of interest.

Received 29 August 2022
Accepted 28 November 2022
Published 21 December 2022

from λ phages from the family *Siphoviridae* (6). PTLBs are nowadays also referred to as tailocins due to their similarity to phages' tails (7, 8). As well as other bacteriocins, phage tail-like bacteriocins evolved as tools for killing other bacteria. Their bactericidal spectra are very narrow; they usually target competing strains within their own species (9, 10).

In general, all R-type PTLBs are very similar in terms of their structural organization, mode of action, and receptor specificity (10–13). The structural organization of the particle consists of a rigid tube, contractible sheath, and a baseplate. The structure appears to be arranged in vertically stacked rings, each consisting of tube and sheath protein hexamers, respectively. Therefore, the particle has an axial 6-fold rotational symmetry (14). The baseplate is located at the distal end of the particle. The tail fibers attached to the baseplate serve as a receptor binding structure-targeting lipopolysaccharide molecules of susceptible bacterial strains (15, 16). The baseplate is the most complex part of the contractile particle and is responsible for initiation of sheath contraction by transferring the signal from tail fibers (17, 18). The R-type tail tube is extended with a spike-shaped protein complex that serves as a membrane-piercing device. An iron ion stabilizes the tip of the spike structure and helps with assembly of the protein complex (19). In general, PTLBs are produced only by a small fraction of bacteria from the whole population; they are assembled inside the cells and released into the environment after cell lysis (10, 20).

Phage tail-like bacteriocins kill the target bacteria by forming a pore. After adsorption on a specific receptor, conformational change in the tail structure follows, resulting in contraction of the sheath and penetration of the tube through the cytoplasmic membrane of the bacterium (21). Data from several studies suggest that even a single PTLB particle is able to mediate cytoplasmic membrane depolarization of the cell (10, 11, 13). The sheath contraction is irreversible, as the contracted sheath is in the final low-energy state; there can be only one attempt to create a membrane pore (22).

For F-type bacteriocins, the mode of their antibacterial action has not been well studied yet, but it seems very likely that the disruption of bacterial envelope and dissipation of membrane potential are involved (23). Production of F-type particles into the medium is very low compared to the R-type bacteriocins (12, 24). Considering this, mostly R-type bacteriocins will be discussed further in this paper.

As the emergence of antibiotic-resistant bacterial pathogens is a persistent worldwide problem and because wide-spectrum antibiotics are no longer an effective solution, phage tail-like bacteriocins are now the subject of research as possible new antimicrobial substances (25, 26) because of their potency, single-hit mode of action (21), and lack of genetic material in contrast to bacteriophages. For the possible therapeutic usage, the narrow antibacterial spectrum of PTLBs could also be a disadvantage. However, this obstacle was solved in pyocins, PTLBs from *Pseudomonas aeruginosa*, by fusing tail fibers of pyocins with parts of tail fibers of bacteriophages that infect different hosts, for example, *Escherichia coli* (27).

This study is targeted at fonticins, phage tail-like bacteriocins produced by at least five strains of the hydrogen sulfide-producing bacterium *Pragia fontium* from the family *Budviciaceae* (28, 29). Spontaneous production of fonticin particles is rather low, and their expression is stimulated in the bacterial population that undergoes certain stress situations. Using mutagenic agents like UV radiation or mitomycin C, bacteriocin production can increase by 2 orders of magnitude (12, 28). It has been shown previously that fonticins kill susceptible strains related to the producing strain, but the bacterium is insensitive to its own bacteriocin (12). Fonticins had been shown to kill susceptible bacterial cells using the same mechanism of contraction and penetration of the bacterial envelope as other PTLBs (12, 30–32).

Despite the fact that PTLBs are expected to create pores in the cytoplasmic membrane of bacterial cells, to the best of our knowledge, no direct observation and detailed investigation of pore formation was carried out so far on artificial membranes. We have conducted this study in order to experimentally verify the pore-forming activity of fonticin particles on living bacterial cells. However, to study the single-pore properties of fonticins, we decided to use the advantage of a simplified bilayer model of

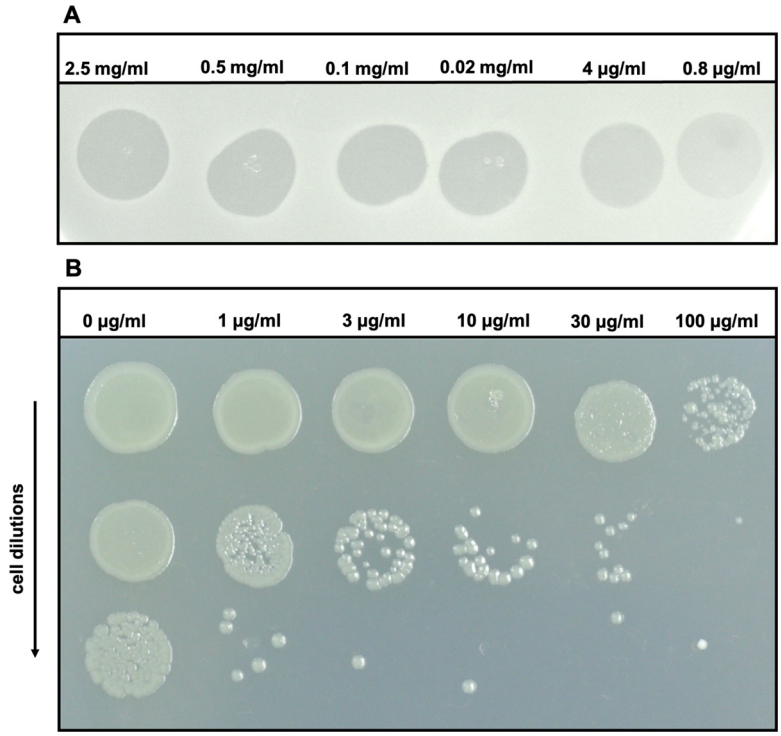

FIG 1 Antimicrobial activity of strain 24613 fonticin particles on a susceptible *Pragia fontium* strain. (A) Fonticin preparation was 5-fold serially diluted (see labels), and 5 μL of each dilution was spotted on LB top agar with susceptible strain of *Pragia fontium* 24647. The highest concentration applied (2.5 mg/mL) corresponds to the original fonticin preparation. The lowest concentration (0.8 μg/mL), which produced a visible spot, is shown. More diluted samples did not inhibit bacterial growth (not shown). Representative results from at least five separate spot tests are presented. (B) Killing activity of fonticin particles shown by cell survival assay. Susceptible cells of *P. fontium* 24647 were 10-fold serially diluted (from OD_{450} of 0.2 to 0.002) and incubated with fonticin particles (24613) with increasing concentrations (0, 1, 3, 10, 30, and 100 μg/mL) and spotted on the LB agar plate directly (3 μL).

black lipid membranes (BLMs), not reflecting the complexity of bacterial envelope but allowing the exact biophysical characterization.

RESULTS

Identification and structure of fonticins. Fonticin particles are produced in the cultivation medium after mitomycin C addition to a growing culture of *Pragia fontium* 24613 (12). After 14 h (20°C, 160 rpm) of induction followed by centrifugation, filtration, and ultracentrifugation, the antibacterial activity of fonticins was tested (see Materials and Methods). Fonticins created clear zones of inhibition on LB agar plates that were overlaid with LB top agar containing the susceptible bacterial strain *Pragia fontium* 24647 (Fig. 1). Inhibition zones made by fonticins typically have sharp edges due to the absence of diffusion in the agar medium, in contrast to most antibiotics and low-molecular-weight bacteriocins, such as microcins (33). Also, the cell survival assay was performed to show fonticin antibacterial activity quantitatively (Fig. 1B).

The production of fonticins was visualized by transmission electron microscopy (TEM). Fonticins were negatively stained by uranyl acetate. Electron micrographs showed (Fig. 2; see Fig. S2 in the supplemental material) that *Pragia fontium* 24613 produces phage tail-like bacteriocins of both R- and F-types, but mainly contractile (R-type) particles were present, in accordance with previous reports (12). We quantified the occurrence of various fonticin forms; the most abundant were contractile particles in their native, uncontracted form (84%). Contracted fonticins also occurred regularly in the medium (10% of all particles). The remainder (2%) were flexible F-type particles and production artifacts (4%): separated tubes, poly-sheath arrangements, and subunits from decomposed particles.

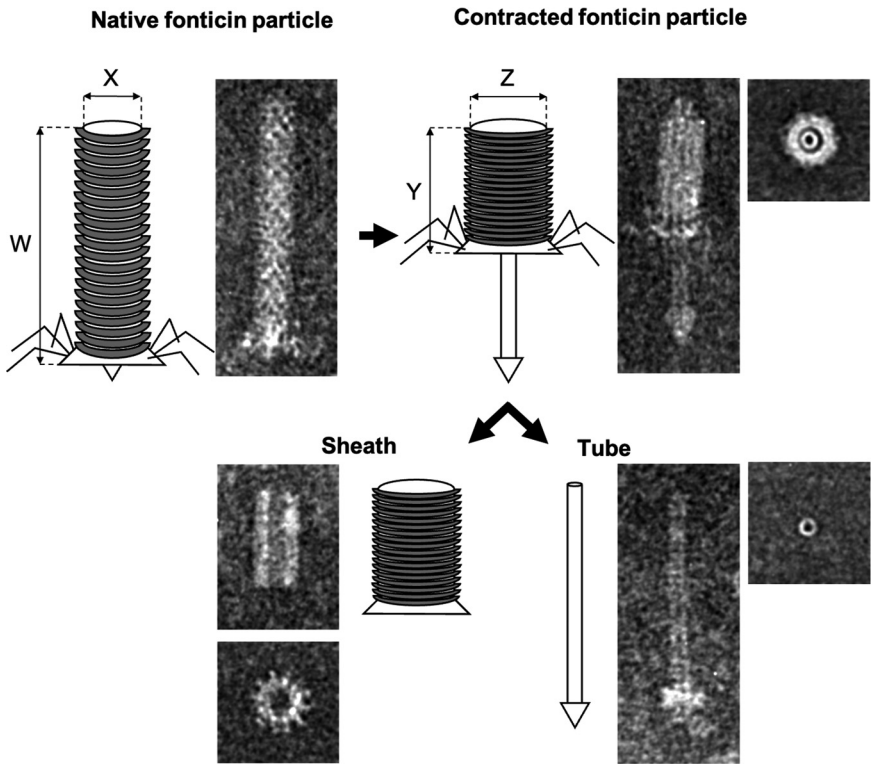

FIG 2 Fonticin contractile particles in their native, contracted, and decomposed forms, with sheath and tube visualized by TEM. The native fonticin particle is 124 nm long (W) and 18 nm wide (X). After attachment of tail fibers to the specific receptor, the sheath is contracted, which enables the tube to perforate cytoplasmic membrane. The contracted sheath is 54 nm long (Y) and 24 nm wide (Z). After contraction, the sheath is usually released from the tube.

Fonticins display the same morphology as other phage tail-like particles (Fig. 2). SDS-PAGE analysis of fonticin particles revealed two major protein bands of 38 and 15 kDa (Fig. S3), corresponding to the sheath and tube subunits detected in related structures, respectively (10, 11). Uncontracted fonticin particles are very uniform in size: they measure 124 $\pm$ 4.5 nm in length and 18 $\pm$ 1.4 nm in width. After contraction, the sheath becomes shorter and thicker (54 $\pm$ 1.5 nm by 24 $\pm$ 1.5 nm) (Fig. 2).

For a more detailed understanding of the fonticin structure, we used two-dimensional (2D) class-averaging analysis of TEM micrographs (Fig. 3) using RELION software. Interestingly, the native particles (Fig. 3A) did not allow the contrasting agent to enter the inner space, as only the sheath is visible on the micrographs. After contraction of the particle, an important change in the fonticin tube occurs: its inner volume is displayed dark, i.e., it is filled by a contrasting agent. This provides evidence that the tube becomes permeant for uranyl acetate (Fig. 3B). From the top views of the tubes (Fig. 3B, highlighted in green and red), we calculated the densitograms (Fig. 3C) and quantified the diameter (d) of the inner fonticin cavity as $d = 4.1 \pm 0.5$ nm. Next, we focused on particle endings in the averaging analysis. For simplicity, we labeled the longer part of the tube protruding through the baseplate *trans* and the opposite part *cis* (Fig. 3B, right). The *cis* side of the tube is bluntly finished and protrudes usually three or four plates out of the sheath. The *trans* side of the tube is more heterogeneous, and it usually carries the spike complex structure (Fig. 3B, right). In less frequent cases, the *trans* side of the tube is also bluntly finished (Fig. S4), or it adheres to sample debris (not shown).

Pore-forming activity of fonticins. The ability of fonticin particles to permeabilize the cytoplasmic membranes of a susceptible bacterial strain was tested on living bacterial cells using potassium efflux assay, which enables direct observation of fonticin pore permeability for inorganic ions. We detected leakage of potassium ions from a

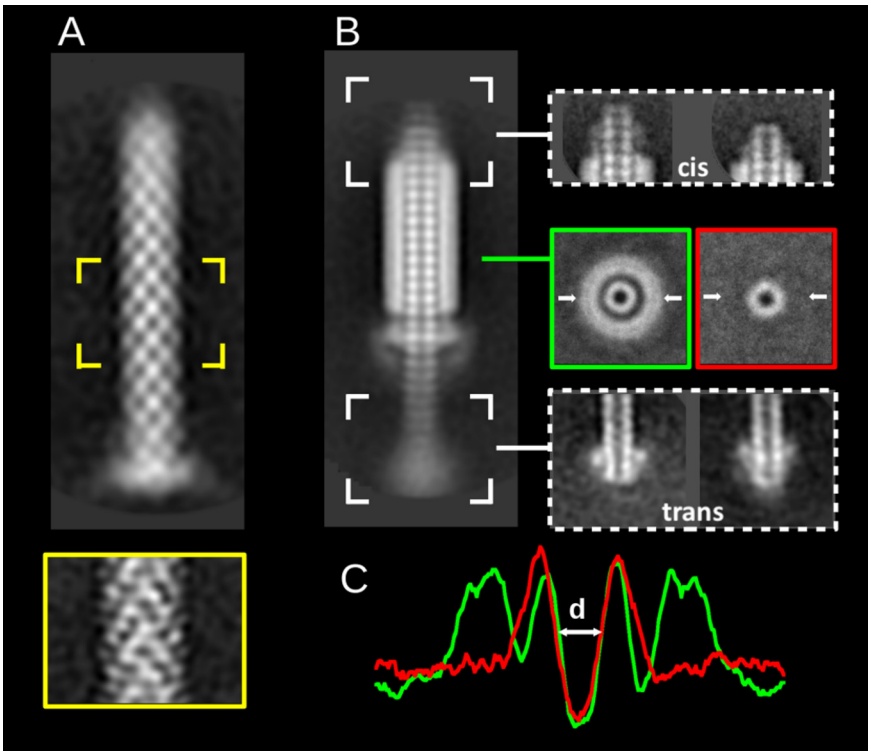

FIG 3 Negative-stain transmission electron micrographs of fonticin particles analyzed by 2D class averaging classification. (A) Fonticin particle in its noncontracted native form (n = 649) and the middle part at a higher resolution (n = 783, highlighted in yellow). (B) Fonticin particle in the contracted form (n = 586) with averaged top view (highlighted in green rectangle) and the top view of separated tube (red rectangle). The top (*cis*) and the bottom (*trans*) ends of contracted particle are shown, both in two representative classes. The white arrows denote the section of diameter quantification. (C) Densitogram used for the quantification of the inner diameter of fonticin particle. The value of d = 4.1 ± 0.5 nm was calculated for the cross-section of the top views.

susceptible strain of *Pragia fontium* 24647 (Fig. 4). After fonticin addition to susceptible cells, within a few minutes, a dose-dependent effect was observed.

(i) Single-pore characteristics. The pore-forming activity of phage tail-like bacteriocins has been known for a long time now, but individual pores have not yet been properly characterized. That led us to perform conductance measurements of individual fonticin pores on black lipid membranes, the model mimicking the biological phospholipid bilayers surrounded by electrolytes. After the addition of fonticins to the BLM system, a steplike increase in electrical current was observed, showing that separated ion-permeable pores were formed probably during incorporation of the fonticin tube into the membrane. Fonticins form mostly stable pores with uniform conductance of about 785 ± 60 pS (Fig. 5A) in standard conditions (1 M NaCl, 10 mM Tris, 8 mM $MgCl_2$, pH 7.3, applied potential 50 mV, membranes made with *E. coli* lipids). Under these conditions, the lifetime of the pore is very long, usually several minutes (data not shown). Each pore is typical, with a considerable current noise.

We measured the single-pore conductance of fonticins in NaCl solutions with increasing molar strength (from 0.1 M to 3 M) and plotted it as a function of NaCl conductivity (Fig. 5B). At NaCl concentrations lower than 0.1 M (data not shown), fonticin particles were less active. The obtained dependence is linear; therefore, fonticin pores are not saturable by Na^+ and Cl^- ions.

Next, we analyzed the ion selectivity of fonticin pore based on reversal potential. The single-pore current measurement was performed in a 10-fold ion concentration gradient across the membrane, with 1 M NaCl on the *cis* and 100 mM NaCl on the *trans* sides, respectively. Both solutions were buffered with 10 mM Tris-HCl to pH 7.3. The applied

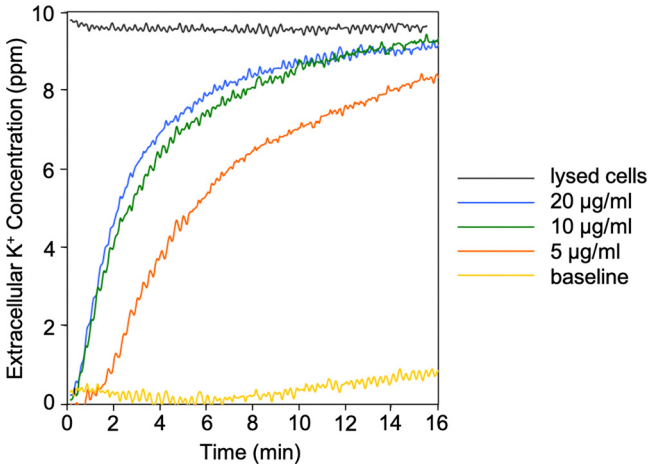

FIG 4 Efflux of potassium ions from living cells due to the rapid pore formation induced by fonticins. Baseline shows untreated cells of *Pragia fontium* 24647. Potassium efflux was measured using potassium-selective electrodes in a vessel containing 6 mL of cell suspension with OD_{450} of 0.2. The maximum potassium efflux was achieved by disruption of all cells by sonication (lysed cells). The data were converted to parts per million. Before each measurement, the calibration of potassium-selective electrodes was measured using precisely defined amounts of KCl solution (0.1, 1, and 10 ppm). The data were aligned to zero by subtracting the initial baseline value. Original values of the baseline and lysed cells were 0.30 and 0.36 V of electrical potential, respectively. Representative results from three separate measurements are shown.

potential was continuously modulated within the interval from −60 to +60 mV. The obtained reversal potential for NaCl, U_{rev} = 0.8 ± 2.2 mV, indicates equal permeability for Na^+ and Cl^- ions (Fig. 5C), with a similar result also for K^+ and Cl^- ions (data not shown). Zero selectivity of fonticin pores to any of the tested ions shows that the transport of these ions is probably not limited by the inner surface of the fonticin pore.

(ii) Mapping the fonticin nanotube by PEG molecules. For characterization of the fonticin pore inner profile, we used polyethylene glycols (PEGs) of various molecular weights. If the molecules of PEG are small enough, they can enter the pore lumen. In that case, PEG blocks the passage of Na^+ and Cl^- ions and limits the electrical current through the membrane. In these experiments, fonticins were added to the *cis* side of the cuvette in a concentration of 50 μg/mL. After several hours of recording baseline and unblocked fonticin pores, we added PEG 1000, 3350, or 8000 (20% [wt/vol]) to the *trans* or the *cis* side of the cuvette, respectively, and recorded altered single-pore currents. We detected blockades of fonticin pores of the two types, decrease of overall ionic current or transient lowering of ionic current with enhanced current noise (Fig. 6). We aimed for average single-pore conductance. The molecules of PEG 1000 were able to enter the fonticin pore from both sides of the membrane, reducing the electrical current to ~40% or ~20% when added from *cis* and *trans* sides, respectively. The addition of PEG 1000 to the *cis* side probably led to disintegration of some fonticin particles to smaller parts (possibly shorter tubes), as we detected frequently atypical high-conductance single-pore events (2.5 nS) (Fig. S5). Next, PEG 3350 molecules were able to block about half of the fonticin particles when added from the *cis* side and reduced the electrical current to ~25%. However, most of the fonticin pores were not blocked by PEG 3350 added from the *trans* side of the membrane. The molecules of PEG 8000 did not induce any significant decrease in fonticin pore current (Fig. 6), suggesting they cannot enter the pore from any side.

DISCUSSION

This study presents pore-forming properties of phage tail-like particles called fonticins, produced by the Gram-negative bacterium *Pragia fontium* 24613. Our data show that *P. fontium* produces R-type fonticins that measure 124 nm, which is within the range recognized for the same fonticin particles previously (12). These dimensions of R-type fonticins are also in agreement with those of many other phage tail-like bacteriocins like pyocins

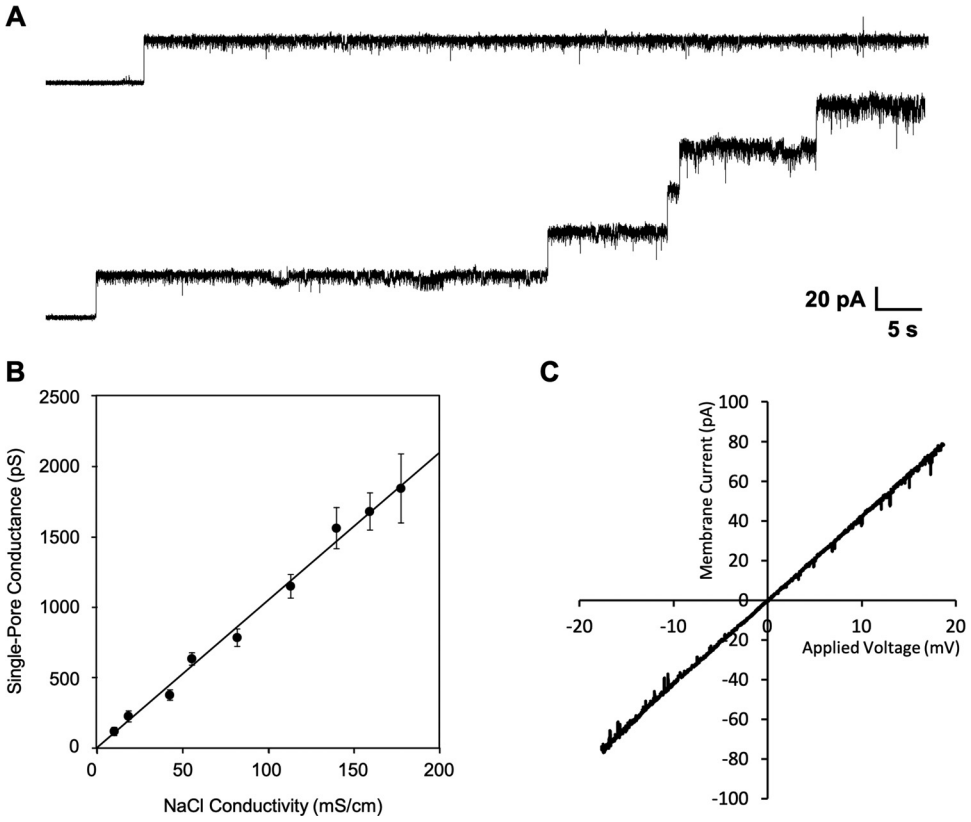

FIG 5 Pore-forming activity of fonticins on black lipid membranes. (A) Example of one open membrane pore and gradual opening of five fonticin pores. With an increasing number of open pores, the current noise increases. The average single-pore conductance is 785 pS (histogram is shown in Fig. 6) measured in standard conditions (1 M NaCl, 10 mM Tris, and 8 mM $MgCl_2$, pH 7.3, with applied voltage of 50 mV). (B) Single-pore conductance of fonticins as a function of NaCl conductivity. Each point corresponds to a pore conductance measured in NaCl solution with increasing molar strength, specifically, 0.1, 0.25, 0.5, 0.75, 1, 1.5, 2, 2.5, and 3 M NaCl. For each NaCl concentration, a conductance histogram ($n > 100$) was constructed and fitted to a Gaussian function. The error bars represent the width at the half maximum of the Gaussian fit. The data points can be fitted to a straight line with a slope of 10.5 pS·cm·mS^{-1}. (C) Current-voltage characteristics of five fonticin channels that were simultaneously present in the membrane with 10-fold NaCl gradient. Ion selectivity for Na^+ and Cl^- ions is 1:1 as can be deduced from the reversal potential where $U_{rev} = -0.8$ mV.

(34) or serracins (32). On the other hand, enterocoliticins were found to be about 35% shorter, although they have similar overall structure (11). We show details of the fonticin structure, namely, the types of tube endings. From TEM images, we can conclude that the fonticin tube becomes permeable for the solvent only after particle contraction. At that moment, the shorter (*cis*) ending opens to the medium, and the other side (*trans*) of the tube bears a membrane-piercing complex that can be spontaneously released even *in vitro*.

The ability of fonticins to kill sensitive bacterial cells is easily verified by a spot test on an agar plate with a sensitive bacterial strain. Fonticins form clear zones of inhibition even in concentrations of 0.8 μg/mL. Due to the large size of fonticin particles, the shape of the zone of inhibition reflects exactly the shape of the applied spot, as fonticins are not able to diffuse through the agar.

We estimated the number of fonticin particles per cell needed for growth inhibition when expecting the molecular mass of fonticin particle to be about 1 MDa and the effective concentration in the range of 1 nM. In the spot test assay, we applied the amount of 2.6×10^8 bacteria (in 0.1-mL suspensions) to the total area of the plate, 53 cm^2. This corresponds to about 4.6 million cells treated with the 5-μL droplet containing 500 million fonticin particles, yielding 150 particles added per cell. At this multiplicity, fonticins kill all bacteria in the suspension. In this respect, fonticins seem less potent than other phage tail-like

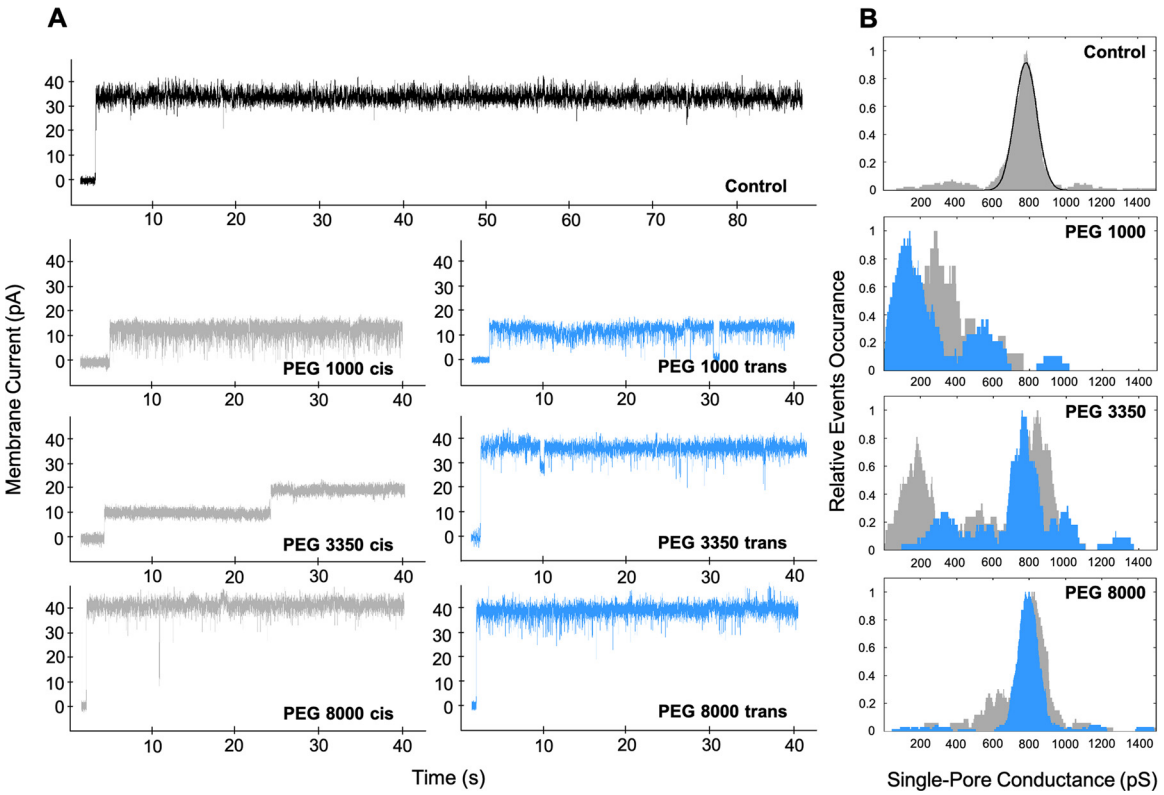

FIG 6 Effect of various sizes of polyethylene glycol on fonticins. (A) Representative current traces of fonticin single pores that were unblocked (control) and blocked by PEG 1000, 3350, and 8000. All measurements were performed at a constant potential of 50 mV in 1 M NaCl, 10 mM Tris, and 8 mM $MgCl_2$, pH 7.3, with *E. coli* lipids. Fonticin pores were blocked by the presence of 20% (wt/vol) PEG 1000, 3350, or 8000, which was added to the *cis* (gray current traces) or *trans* (blue current traces) side of the cuvette. (B) For each PEG size and side of PEG addition (*cis* or *trans*), a conductance histogram ($n > 60$) was constructed using kernel density estimation (rectangular kernel with 50 pS width). The *cis* side addition of PEG is shown in gray and the *trans* side addition in blue. The control histogram of unblocked fonticin pores was fitted to a Gaussian function with its center at 785 pS.

bacteriocins like pyocins. We expect that the relatively low killing activity of our fonticin preparations could be caused by less effective binding to the treated cells or spontaneous contraction of particles during their addition.

Pragia fontium 24613 produces both types of fonticins (R- and F-types); both theoretically might form membrane pores. To confirm that the R-type particles have a major effect on pore formation, we used the strain *P. fontium* 25240, which is also able to produce R-type fonticins but cannot produce F-type particles, as confirmed by TEM observations (see Fig. S6 in the supplemental material). Fonticins produced by strain *P. fontium* 25240 form less frequent but standard pores on BLM (Fig. S7), with a single-pore conductance of 904 $\pm$ 75 pS. We did not use fonticins produced by strain 25240 in our experiments, as these fonticins are more likely to contract themselves spontaneously, so the detected frequency of pore formation is quite low. We conclude that in our experiments, the pore-forming activity of fonticin particles is very likely mediated only by R-type fonticins. We still cannot completely exclude certain pore-forming activity of F-type fonticins of strain 24613. However, we can conclude that fonticins produced by strain 24613 show comparable pore properties to R-type particles of strain 25240 in our experimental setup. To the best of our knowledge, the producer strain of solely F-type fonticins has not been discovered nor constructed yet, so we cannot test the possibility of specific pore formation by F-type particles.

We are aware of the risks involved in the use of rough extracts in the production of fonticin particles. These preparations may certainly contain other components that could theoretically be also responsible for the formation of certain membrane pores. Such proteins could include, for example, parts of disassembled particles like tape

measure protein (TMP; required to determine the length of tail). In fact, the role of TMP in disrupting the bacterial inner membrane was already described in *Myoviridae* (23, 35, 36). However, the soluble TMP from *P. fontium* would lose its long tubular form; thus very high single-pore conductance could be expected in contrast to the conductance of a long cylindrical fonticin tube. Such an effect was observed with isolated TMP (pb2 protein) from T5 virus showing high single-pore conductance of 4.6 nS in 1 M KCl (37). Other contaminants not related to bacteriocins (like the OmpA protein) can be rarely present in the fonticin extract and are also known to interact with artificial membranes (38).

To exclude the possibility that pore formation is due to individual protein contaminants, genetic manipulation would have to take place. Deletion or inactivation of responsible genes in a wild isolate is complicated by the presence of several gene clusters possibly involved in the expression of R-type fonticin protein components (Fig. S8). Moreover, the intentional elimination of a particular single component followed by loss of pore-forming activity would lead to ambiguous conclusions. It might be explained by (i) direct involvement of the deleted protein in membrane disruption, or (ii) misassembly of the whole fonticin particle. An alternative approach would be heterologous expression of individual relevant proteins in a strain that is unable to produce any kind of bacteriocins.

However, in our experiments, the internal pore diameter determined using nonelectrolytes and Ohm's law corresponds well to the expected fonticin particle diameter (according to TEM and literature). Therefore, we assume that possible contaminating components did not have a significant effect on pore formation in our results.

We have demonstrated that R-type fonticins (produced by *P. fontium* 24613) form pores in the cytoplasmic membrane of susceptible bacterial cells and they are also able to form large pores in the artificial membranes composed of isolated *E. coli* lipids. The pore-forming activity of fonticins *in vivo* was measured using potassium leakage assay. The kinetics of lysis measured by K^+ efflux (Fig. 4) starts within seconds even after the smallest amount of fonticin addition (5 μg/mL), exhibiting almost no time delay, which might suggest single-hit kinetics (39). The K^+ efflux correlates with decay of living bacteria according to cell survival assay (Fig. 1B) where even the lowest concentrations of fonticins added to a susceptible strain, 24647, are able to kill bacterial cells.

In vitro fonticin pore characteristics were provided by conductance measurements on the black lipid membranes. Our results clearly show that fonticins form distinct nonselective pores with very stable conductance of 785 pS that linearly depends on the molar strength of the buffer used. *In vivo*, fonticins are expected to form these large transmembrane pores during contraction of their sheath after binding on specific receptors, probably a lipopolysaccharide of specific composition, on the surface of sensitive bacterial cells. Fonticins are able to form pores even with no LPS present in the black lipid membranes formed with *E. coli* lipids dissolved in *n*-decane and butanol. However, a similar effect is seen routinely with other pore-forming agents like bacterial toxins (ApxIA, CyaA, or RtxA) that do not require their native receptors in BLM experiments (40–43). Such an effect can be explained by specific features of the used method; only those molecules/particles that are inserted properly into the planar lipid bilayer and form a transmembrane pore can be selectively detected, although they are surrounded by a vast majority of nonbounded molecules (44). The presence of a specific membrane receptor usually induces dramatically enhanced binding and insertion of studied molecules into the bilayer followed by increased membrane permeability. But the presence of membrane receptors showed only a negligible effect on specific pore properties like typical single-pore conductance, pore stability, or ion selectivity of bacterial toxin CryIAa (45).

Although fonticins bind to the surface of artificial membranes with less efficiency, just a few molecules per hour, we are still able to detect their pores due to the sensitivity of the method. It is not clear whether fonticin particles bind to the surface of the artificial membrane and form pores during the contraction of their sheath, as in the case of living bacterial cells, or if the precontracted particle is also able to create the pore

into the artificial membrane. There is also an option that tubes that are separated from their sheaths could also be responsible for pore formation on artificial lipid membranes. In this case, we would anticipate similar single-pore properties of separated tubes and the whole fonticin particle because of their identical expected pore diameter and profile.

The dependency of conductance of fonticin pores on the NaCl concentration (or conductivity) is linear, with a slope of 0.69 pS · mM^{-1}. Such a specific pore conductance means that every increase of NaCl concentration by 1 mM increases the conductance of fonticin pore by ~0.7 pS. From such pore behavior, together with no ion selectivity (Fig. 5), we deduce that the inner shape of the channel can be plausibly approximated by a rigid cylinder filled with the electrolyte. In line with this premise, we estimated the effective inner diameter of the fonticin pore using calculation of cylindrical shape conductor properties $G = S/(\rho \cdot l)$, where G stands for conductance of fonticin pore that is 0.78 nS in 1 M NaCl (Fig. 5), l is the length of the conductor where l = 124 nm (known from the TEM images shown in Fig. 2), S is the conductor cross section, and ρ is specific electrical resistivity where ρ = 117,647 $\mu\Omega$m (for simplification, calculated from conductivity of NaCl solution; χ = 85 mS/cm). From these values, we obtained S = 11.45 nm^2, yielding the effective inner diameter of fonticin pore of d_{eff} = 3.82 nm, calculated for Na^+ and Cl^- ions without any substantial interaction of these ions with the wall of the pore. To compare our result with another pore-forming protein complex, we calculated the inner diameter also for α-hemolysin from *Staphylococcus aureus* using the same equation. The conductance of α-hemolysin was 0.69 nS, measured under the same conditions as fonticins (1 M NaCl, applied potential 50 mV; data not shown). Our calculation suggests that the effective inner diameter of α-hemolysin is 1.0 nm (expecting that the length of the pore, l, is 9.8 nm) (46). Crystallographic data reveal that α-hemolysin's real inner diameter is considerably larger and ranges from 1.4 to 4.6 nm. There is a discrepancy between the effective inner diameter of α-hemolysin pore and crystallographic model, which shows that α-hemolysin cannot be simply approximated by a cylindrical conductor. Fonticin nanopore has ~14 times larger effective pore cross section but 13 times longer particles than α-hemolysin (46) (Fig. 2), which explains comparable overall ion conductance of these nanopores.

The usual procedure for determining the pore size is to block single pores with different sizes of nonelectrolytes, e.g., polyethylene glycols (47, 48). However, the size and shape of PEG molecules are still a matter of research. One could expect random or Gaussian chains, stretched forms, and helical or planar structures (49), which might complicate the interpretation of the data. We tested if PEG 1000, 3350, or 8000 is able to enter into the fonticin pore from the *cis* and *trans* sides of the membrane and alter the single-pore properties (Fig. 6). We expect that the fonticin tube binds to the artificial membrane by its *trans* ending (labeled in Fig. 3B; BLM scheme in Fig. S1), which is supposed to carry a membrane-piercing complex. PEG 1000 molecules that have a diameter of about 1.88 nm (42) induced considerable fonticin pore blocking when added from any side of the membrane. However, PEG 3350 molecules with an average size of 3.56 nm (42) were able to enter the fonticin pore mostly from the *cis* side. The majority of recorded fonticin particles with PEG 3350 added to the *trans* side did not show decreased single-pore conductance. From this observation, we speculated that the *cis* end of the particles remains open and accessible for the molecules in the solution, whereas the *trans* end is partially closed by the spike complex that still allows the passage of Na^+ and Cl^-. Interestingly, for a few fonticin molecules, we also observed blocking by PEG 3350 from the *trans* side. We suppose that these were the particles with released spike complexes, as can be rarely observed also on TEM images (Fig. S4). The largest nonelectrolyte tested, PEG 8000, did not block the fonticin pore from any side of the membrane. We estimate the molecular diameter of PEG 8000 to be 4.50 nm based on published data (50).

The ability of PEG molecules to block fonticin pores was, in fact, surprisingly high. The bulk conductivity of the electrolytes with PEG (20% [wt/vol]) was approximately

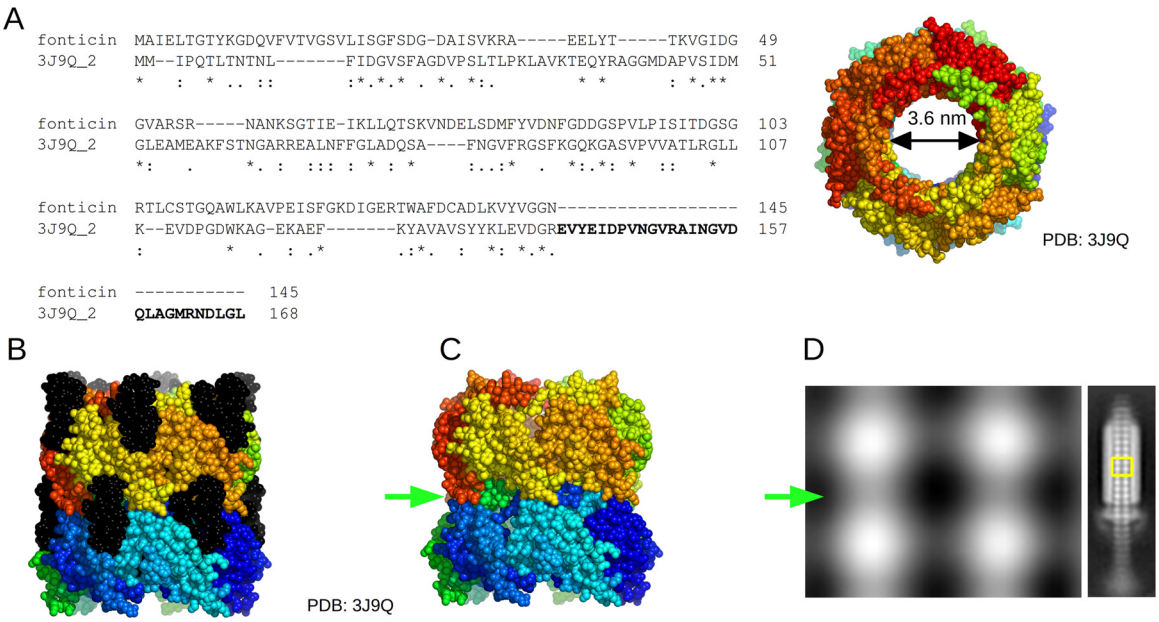

FIG 7 Comparison of fonticin major tube protein and related pyocin tube protein. (A) Sequence alignment of fonticin major tube protein (QQ39_04825) and pyocin tube protein (GenPept accession no. WP_003085175; PDB accession no. 3J9Q) from *Pseudomonas aeruginosa* (14). The sequence alignment was performed by Clustal Omega (1.2.4) software. The C-terminal part of the pyocin protein sequence (in bold) is missing in the fonticin sequence. On the right side, the tube structure is shown with a highlighted inner diameter of about 3.6 nm. (B) Side view of reconstructed pyocin tube structure. The parts highlighted in black correspond to the C terminus of the protein missing in the fonticin structure. (C) Model of pyocin tube structure with removed C-terminal 29-amino-acid residues to mimic the situation in fonticin. These residues are clearly responsible for interaction of the pyocin tube with the sheath and for stabilizing the tube stacks above each other. When the C-terminal part of the tube protein is missing, then clear necking (green arrow) of the whole tube can be seen. The images were generated using PyMOL software. (D) Averaged 2D model of fonticin tube (TEM images from Fig. 3) showing separated stacks with necking (green arrow). Similar necking can be seen in bacteriophage φ812K1-420 (52).

43 mS · cm^{-1} for all types of PEG molecules in contrast to pure 1 M NaCl with conductivity of 86.3 mS · cm^{-1}. From these values, one would expect about a 50% decrease in pore current if the inner channel volume stays occupied by PEG molecules compared to bulk solution. As the blocked pore conductance for PEG 1000 and 3350 is between 20 and 40% (of the unblocked pore), we can conclude that PEG molecules tend to accumulate within the fonticin pore. A similar effect was already observed in, e.g., hemolysin BL, enterotoxin of *Bacillus cereus* (51).

We characterized the fonticin tube shape also by TEM densitograms and quantified the inner diameter of about 4.1 nm ± 0.5 nm. Note that the absolute value depends on the selected criteria because the contrasting agents accumulate inside the tubes more than in the surroundings (Fig. 3C). All these results are also consistent with the dimensions of related structures that were experimentally solved (14, 52) (PDB ID accession no. 3J9Q) where we recognized an inner diameter of about 3.6 nm (Fig. 7).

This inner tube diameter clearly evolved to allow the transport of double-stranded DNA through the bacteriophage tail. Another established function of the inner tube of both R-type bacteriocins and phage tails is to house the tape measure protein, which fills the internal space of the tube, as can be seen in some of the higher resolved cryo-electron microscopy (cryo-EM) structures (3, 53). Later, the structure changed its function, as the fonticin particles effectively kill the sensitive cells by perforating their membranes for small ions and molecules. If we reflect that potassium and chloride can freely pass through to the contracted phage tail-like bacteriocins, which leads to cell death very effectively, then we came across an intriguing notion. The evolutionarily related contractile tail bacteriophages must have their capsid head sealed waterproof, not only to protect its genome from environmental stressors but also to prevent killing the phage's host cell, as bacteriophages need theirs hosts alive. Any potential mutation

in bacteriophage capsid that would cause ion flux across the bacterial membrane would be doomed to evolutionary failure and extinction.

Pore-forming proteins embedded into the artificial lipid membranes have already been tested for detection, characterization, and quantification of various types of molecules. Lots of the work has been done on α-hemolysin (from *Staphylococcus aureus*) (54) or *Mycobacterium smegmatis* porin MspA (55, 56). Both of them became the model protein pores for both nanopore-based mass spectroscopy in solution (54, 57) and DNA sequencing by nanopore (58, 59). Both methods are based on quantification of changes in ionic current. We propose that R-type fonticin particles might be used for characterization of double-stranded nucleic acids in solution in terms of their length and possibly secondary structure. The only essential complication stems from the necessity to quantitatively remove the terminal membrane-piercing complex from the tube. We demonstrated *in vitro* that this complex is permeable for small ions but not for molecules larger than 3 kDa (Fig. 6). We hypothesize that this complex may stay preserved in the fonticin particles perforating the attacked cell. If so, the complex shape and the nature of its surface ensure a firm attachment of the particle in the membrane, but it can also serve as a kind of filter protecting fonticin from clogging by cellular protein molecules.

Conclusion. The aim of the presented research was to examine the structure and pore-forming activity of fonticins, phage tail-like bacteriocins produced by *Pragia fontium*. We have demonstrated that fonticins perforate bacterial membranes and induce K^+ efflux. At the same time, these bacteriocins create defined pores in the artificial lipid membranes. We assume that both phenomena are induced by the same types of structures. The conductance of fonticin pore in artificial membranes is 785 pS in 1 M NaCl and is linearly dependent on the molar strength of electrolyte used. By calculation of cylindrical shape conductor properties, we deduced the effective inner diameter of fonticin pore to be 3.82 nm, which is in agreement with our data from transmission electron microscopy, where the tube diameter was recognized to be about 4.1 nm. The largest PEG molecule that can enter the tube has a diameter of about 3.56 nm, whereas the PEG molecule of 4.5 nm cannot pass the pore. The terminal membrane-piercing complex also restricts the molecules entering the fonticin tube. In the possible use of fonticins in mass spectroscopy in solution, the wide inner diameter of the pore could be advantageous for detecting larger molecules like dsDNA or dsRNA.

MATERIALS AND METHODS

Bacterial strains and growth conditions. In this work, the following bacterial strains were used. *Pragia fontium* 24613 was the strain producing fonticins. *Pragia fontium* 24647 was used as a strain susceptible to fonticins produced by the strain 24613, but it is also able to produce its own fonticin particles. *Pragia fontium* 25240 was used as another strain producing fonticins. All bacterial strains were kindly donated by Jan Šmarda and previously characterized (12). The bacterial strains were grown aerobically in LB medium at 30°C. The growth was monitored by measuring optical density at 450 nm (OD_{450}).

Production of fonticins. The protocol for PTLB production was described previously (11) and adjusted for fonticins. Fonticin production by the producing strains (*P. fontium* 24613, 24647, or 25240) was induced by 0.5 μg/mL mitomycin C (Carl Roth) as addition to a growing culture (OD_{450} = 0.5, 30°C, 160 rpm). After 14 h of incubation (20°C, 160 rpm) the cells were pelleted (8,000 $\times$ *g*, 30 min, 4°C), and supernatants were sterilized by filtration (MF-Millipore membrane filter; 0.22 μm pore size). Sterilized supernatants were treated with 0.8 mM Triton X-100 to solubilize contaminating membrane vesicles. After 1 h of incubation with Triton X-100, supernatants were pelleted by ultracentrifugation (28,000 $\times$ *g*, 2 h, 4°C). Pellets were then resuspended in a buffer containing 150 mM NaCl, 8 mM $MgCl_2$, and 10 mM Tris (pH 7.2) to a concentration of 2.5 mg/mL. The concentration of fonticins was determined by Bradford protein assay, and the sample quality was controlled by SDS-PAGE. To remove unwanted residues of bacterial DNA, DNase (DNase I from bovine pancreas; Roche) was added to each fonticin preparation at a concentration of 200 μg/mL, followed by incubation at 37°C for 2 h. For our purposes, fonticins were not further purified because every such attempt led to a considerable loss of activity. The antimicrobial activity of each fonticin preparation was examined by a spot test.

The majority of experiments were performed with fonticins produced by strain 24613. Fonticins in this paper are meant the ones from *P. fontium* 24613 if not specified otherwise.

Antimicrobial activity of fonticins. (i) Spot test. Fonticins (2.5 mg/mL) were serially diluted with sterile distilled water, and 5 μL of each dilution was applied on the LB plates topped with 3 mL of LB top agar containing 100 μL of susceptible bacterial culture in the exponential phase (OD_{450} = 0.6, which is about 2.6 $\times$ 10^9 CFU/mL). Plates were incubated overnight at 30°C.

(ii) Cell survival assay. The cell survival assay was performed as described previously (27, 60) with a

few modifications. Susceptible bacterial cells (60) of *Pragia fontium* 24647 were harvested by centrifugation at the exponential phase (O D_{450} = 0.5) and resuspended in 10 mM HEPES buffer (pH 7.3) with 0.5% glucose to an optical density of OD_{450} of 0.2. Susceptible cells were subsequently 10-fold serially diluted to OD_{450} of 0.02 and 0.002. Fonticins (24613) with increasing concentrations of 0, 1, 3, 10, 30, and 100 μg/mL were incubated in LB with susceptible bacterial cells (*P. fontium* 24647) for 15 min at 30°C. The samples (3 μL) were then applied on the LB agar plate and incubated overnight at 30°C.

K^+ efflux assay. Measurements of potassium efflux using living cells were performed as described previously (61). Briefly, *Pragia fontium* 24647 cells were grown aerobically overnight at 30°C. Overnight culture was used to inoculate LB medium (starting density, OD_{450} = 0.05) enriched with 10 mM KCl. Cells were grown until the exponential phase was reached (OD_{450} = 0.5) and then harvested by centrifugation at 5,000 $\times$ *g*, 25°C, for 10 min. The cell pellet was washed in 100 mM sodium phosphate, pH 7.0, and then resuspended in 1 mL of 100 mM sodium phosphate, pH 7.0, with 5% glycerol (assay buffer). Cells were kept on ice and used within 2 h after 30 min of incubation on ice. An aliquot of cells was added to a K^+ efflux cuvette containing assay buffer (the temperature was maintained at 30°C) to a final OD_{450} of 0.2. Potassium efflux measurements were performed using an ion-selective electrode for potassium ions (Elit 8031 with a polyvinyl chloride [PVC] membrane), double-junction lithium acetate reference electrode (ELIT 003n), and a temperature probe. As a baseline, an amount of potassium ions leaked from untreated cells was recorded for all experiments. Fonticins were added at concentrations of 5, 10, and 20 μg/mL. As a positive control, the cells were lysed by sonication, exerting a maximum possible K^+ efflux. Prior to all of the measurements, the electrodes were calibrated by measuring a series of K^+ standards (0.1, 1, and 10 ppm KCl).

Transmission electron microscopy. Fonticins (0.5 mg/mL) were applied on a carbon-coated copper grid and removed after 5 min by a wedge of filter paper. The grid was then washed three times with distilled water. After the fonticin suspension had dried, the negative stain was performed two times (30 s each) with a fresh, filtered solution of 2% (wt/vol) uranyl acetate. Samples were visualized with a Jeol JEM-2100Plus electron microscope at 120 kV (Imaging Methods Core Facility, Biocev, Prague, Czech Republic).

The occurrence of fonticins in all of the different types and conformations was calculated manually using negatively stained fonticin preparation (*n* = 1,274 particles analyzed). The quantification of fonticin dimensions in native and contracted conformation (*n* = 98) was performed manually using Fiji (ImageJ 2.1.0/1.53c) software.

For the purpose of image analysis by 2D class averaging, about 2,000 transmission electron micrographs of negatively stained fonticins (0.5 mg/mL) were collected by Tecnai F20 (200 kV, Cs objective 2.0 mm) with a magnification of 62,000$\times$ (1.79 Å/pixel). Two-dimensional class averaging classification was provided by EMAN2 (version 2.31) and RELION (version 3.1.2) software (Cryo-electron Microscopy and Tomography of CIISB [CEITEC], Brno, Czech Republic).

Black lipid membranes. Electric current measurements were performed in a Teflon cuvette divided into two compartments by a Teflon partition with a small aperture (0.5 mm in diameter) in it, connecting both compartments. Each compartment was filled with 1.5 mL of 1 M NaCl, 10 mM Tris-HCl, and 8 mM $MgCl_2$ (pH 7.2). Black lipid membranes were formed with 3% *E. coli* polar lipids (Avanti Polar Lipids; extract of *E. coli* B [ATCC 11303] containing 67% phosphatidylethanolamine [PE] [wt/wt], 23.2% phosphatidylglycerol [PG] [wt/wt] and 9.8% cardiolipin [CL] [wt/wt], according to the manufacturer) dissolved in *n*-decane/butanol (9:1 [vol/vol]) by painting the lipids across the aperture. The details of this method were described elsewhere (62). Fonticins were added to the *cis* side compartment (the side with the positive electrode) at a concentration of 50 μg/mL (see Fig. S1 in the supplemental material). The membrane potential (50 mV) was maintained using Ag/AgCl electrodes. Electric current was amplified with the LCA-200-10GV amplifier (Femto) and digitized with a KPCI-3108 card (Keithley) at a 2-kHz sampling rate. Single-pore events were analyzed with QuB software (63) and custom-made scripts (64). The conductance of each pore opening was calculated as $G = I/U$, where I is the electric current and U is the membrane potential. Fonticin channels were blocked by PEG 1000 (20% [wt/vol]; Sigma), PEG 3350 (20% [wt/vol]; Sigma), and PEG 8000 (20% [wt/vol]; Sigma); all of the analytes were added to the *cis* or *trans* side of the cuvette, depending on the experimental setup.

The ion selectivity of fonticin channels was measured using triangular voltage ramps for a period of 100 s. Applied potential ranged from -60 mV to 60 mV and was changing linearly. The ion selectivity was measured in a 10-fold ion gradient, with 1 M NaCl (or 1 M KCl) on the *cis* side and 100 mM NaCl (or 100 mM KCl) on the *trans* side; all solutions were buffered with 10 mM Tris-HCl to pH 7.2 and contained 8 mM $MgCl_2$. Salt bridges were used on the electrodes. Fonticins at a concentration of 50 μg/mL were added to the *cis* side of the cuvette. Individual pore openings, plotted as current-voltage dependence, were fitted with a linear function. Obtained parameters were used for calculation of reversal potential (U_{rev}), indicating the applied transmembrane voltage at which the net ion current has a zero value in the presence of ionic gradient across the channel (65). The ion selectivity (Na^+/Cl^- or K^+/Cl^-) was determined as a ratio of ion permeabilities according to the modified Goldman-Hodgkin-Katz equation (66).

$$U_{\text{rev}} = \frac{RT}{F} \cdot \ln \frac{P_c \cdot c_2 + P_a \cdot c_1}{P_c \cdot c_1 + P_a \cdot c_2}$$

where R is the gas constant, T is the thermodynamic temperature, F is the Faraday's constant, P_c and P_a are ratios of permeability of cations and anions, and c_1 and c_2 are concentrations of buffers used on the *cis* and *trans* sides, respectively.

LC-MS. Liquid chromatography-mass spectrometry (LC-MS) analyses were performed in the Laboratory of Mass Spectrometry at Biocev research center; Faculty of Science, Charles University.

SUPPLEMENTAL MATERIAL

Supplemental material is available online only.

SUPPLEMENTAL FILE 1, PDF file, 3.6 MB.

ACKNOWLEDGMENTS

This work was supported by the grant GAUK 1360218 from Charles University to K.L., SVV project 260568 to K.L., the ERDF grant 18_046/0016045 to L.M., and Ministry of Education, project number LM2018129 Czech-BioImaging in cooperation with Imaging Methods Core Facility, Biocev.

We also acknowledge Cryo-electron Microscopy and Tomography of CIISB (CEITEC), Instruct-CZ Centre, supported by MEYS CR (LM2018127).

We thank Lucie Jánská for excellent technical support.

REFERENCES

1. Leiman PG, Kanamaru S, Mesyanzhinov VV, Arisaka F, Rossmann MG. 2003. Structure and morphogenesis of bacteriophage T4. Cell Mol Life Sci 60:2356–2370. https://doi.org/10.1007/s00018-003-3072-1.
2. Basler M, Pilhofer M, Henderson GP, Jensen GJ, Mekalanos JJ. 2012. Type VI secretion requires a dynamic contractile phage tail-like structure. Nature 483:182–186. https://doi.org/10.1038/nature10846.
3. Jiang F, Li N, Wang X, Cheng J, Huang Y, Yang Y, Yang J, Cai B, Wang Y-P, Jin Q, Gao N. 2019. Cryo-EM structure and assembly of an extracellular contractile injection system. Cell 177:370–383.e15. https://doi.org/10.1016/j.cell.2019.02.020.
4. Leiman PG, Basler M, Ramagopal UA, Bonanno JB, Sauder JM, Pukatzki S, Burley SK, Almo SC, Mekalanos JJ. 2009. Type VI secretion apparatus and phage tail-associated protein complexes share a common evolutionary origin. Proc Natl Acad Sci U S A 106:4154–4159. https://doi.org/10.1073/pnas.0813360106.
5. Ge P, Scholl D, Prokhorov NS, Avaylon J, Shneider MM, Browning C, Buth SA, Plattner M, Chakraborty U, Ding K, Leiman PG, Miller JF, Zhou ZH. 2020. Action of a minimal contractile bactericidal nanomachine. Nature 580:658–662. https://doi.org/10.1038/s41586-020-2186-z.
6. Nakayama K, Takashima K, Ishihara H, Shinomiya T, Kageyama M, Kanaya S, Ohnishi M, Murata T, Mori H, Hayashi T. 2000. The R-type pyocin of Pseudomonas aeruginosa is related to P2 phage, and the F-type is related to lambda phage. Mol Microbiol 38:213–231. https://doi.org/10.1046/j.1365-2958.2000.02135.x.
7. Ghequire MGK, De Mot R. 2015. The tailocin tale: peeling off phage tails. Trends Microbiol 23:587–590. https://doi.org/10.1016/j.tim.2015.07.011.
8. Ghequire MGK, De Mot R. 2014. Ribosomally encoded antibacterial proteins and peptides from Pseudomonas. FEMS Microbiol Rev 38:523–568. https://doi.org/10.1111/1574-6976.12079.
9. Dykes GA. 1995. Bacteriocins: ecological and evolutionary significance. Trends Ecol Evol 10:186–189. https://doi.org/10.1016/s0169-5347(00)89049-7.
10. Michel-Briand Y, Baysse C. 2002. The pyocins of Pseudomonas aeruginosa. Biochimie 84:499–510. https://doi.org/10.1016/S0300-9084(02)01422-0.
11. Strauch E, Kaspar H, Schaudinn C, Dersch P, Madela K, Gewinner C, Hertwig S, Wecke J, Appel B. 2001. Characterization of enterocoliticin, a phage tail-like bacteriocin, and its effect on pathogenic Yersinia enterocolitica strains. Appl Environ Microbiol 67:5634–5642. https://doi.org/10.1128/AEM.67.12.5634-5642.2001.
12. Šmarda J, Benada O. 2005. Phage tail-like (high-molecular-weight) bacteriocins of Budvicia aquatica and Pragia fontium (Enterobacteriaceae). Appl Environ Microbiol 71:8970–8973. https://doi.org/10.1128/AEM.71.12.8970-8973.2005.
13. Yao GW, Duarte I, Le TT, Carmody L, LiPuma JJ, Young R, Gonzalez CF. 2017. A broad-host-range tailocin from Burkholderia cenocepacia. Appl Environ Microbiol 83:e03414-16. https://doi.org/10.1128/AEM.03414-16.
14. Ge P, Scholl D, Leiman PG, Yu X, Miller JF, Zhou ZH. 2015. Atomic structures of a bactericidal contractile nanotube in its pre- and postcontraction states. Nat Struct Mol Biol 22:377–382. https://doi.org/10.1038/nsmb.2995.
15. Köhler T, Donner V, van Delden C. 2010. Lipopolysaccharide as shield and receptor for R-pyocin-mediated killing in Pseudomonas aeruginosa. J Bacteriol 192:1921–1928. https://doi.org/10.1128/JB.01459-09.
16. Ikeda K, Egami F. 1973. Lipopolysaccharide of Pseudomonas aeruginosa with special reference to pyocin R receptor activity. J Gen Appl Microbiol 19:115–128. https://doi.org/10.2323/jgam.19.115.
17. Buth SA, Shneider MM, Scholl D, Leiman PG. 2018. Structure and analysis of R1 and R2 pyocin receptor-binding fibers. Viruses-Basel 10:427. https://doi.org/10.3390/v10080427.
18. Taylor NMI, Prokhorov NS, Guerrero-Ferreira RC, Shneider MM, Browning C, Goldie KN, Stahlberg H, Leiman PG. 2016. Structure of the T4 baseplate and its function in triggering sheath contraction. Nature 533:346–352. https://doi.org/10.1038/nature17971.
19. Browning C, Shneider MM, Bowman VD, Schwarzer D, Leiman PG. 2012. Phage pierces the host cell membrane with the iron-loaded spike. Structure 20:326–339. https://doi.org/10.1016/j.str.2011.12.009.
20. Jacob F. 1954. Induced biosynthesis and mode of action of a pyocine, antibiotic produced by Pseudomonas aeruginosa. Ann Inst Pasteur (Paris) 86:149–160. (In French.).
21. Uratani Y, Hoshino T. 1984. Pyocin R1 inhibits active transport in Pseudomonas aeruginosa and depolarizes membrane potential. J Bacteriol 157:632–636. https://doi.org/10.1128/jb.157.2.632-636.1984.
22. Brackmann M, Nazarov S, Wang J, Basler M. 2017. Using force to punch holes: mechanics of contractile nanomachines. Trends Cell Biol 27:623–632. https://doi.org/10.1016/j.tcb.2017.05.003.
23. Scholl D. 2017. Phage tail–like bacteriocins. Annu Rev Virol 4:453–467. https://doi.org/10.1146/annurev-virology-101416-041632.
24. Kuroda K, Kageyama M. 1979. Biochemical properties of a new flexuous bacteriocin, pyocin-F1, produced by Pseudomonas aeruginosa. J Biochem 85:7–19. https://doi.org/10.1093/oxfordjournals.jbchem.a132332.
25. Gebhart D, Lok S, Clare S, Tomas M, Stares M, Scholl D, Donskey CJ, Lawley TD, Govoni GR. 2015. A modified R-type bacteriocin specifically targeting Clostridium difficile prevents colonization of mice without affecting gut microbiota diversity. mBio 6:e02368-14. https://doi.org/10.1128/mBio.02368-14.
26. Damasko C, Konietzny A, Kaspar H, Appel B, Dersch P, Strauch E. 2005. Studies of the efficacy of enterocoliticin, a phage-tail like bacteriocin, as antimicrobial agent against Yersinia enterocolitica serotype O3 in a cell culture system and in mice. J Vet Med B Infect Dis Vet Public Health 52:171–179. https://doi.org/10.1111/j.1439-0450.2005.00841.x.
27. Williams SR, Gebhart D, Martin DW, Scholl D. 2008. Retargeting R-type pyocins to generate novel bactericidal protein complexes. Appl Environ Microbiol 74:3868–3876. https://doi.org/10.1128/AEM.00141-08.
28. Šmarda J. 1987. Production of bacteriocin-like agents of Budvicia aquatica and Pragia fontinum. Zentralbl Bakteriol Mikrobiol Hyg A 265:74–81. https://doi.org/10.1016/S0176-6724(87)80154-2.
29. Adeolu M, Alnajar S, Naushad S, Gupta RS. 2016. Genome-based phylogeny and taxonomy of the 'Enterobacteriales': proposal for Enterobacterales ord. nov. divided into the families Enterobacteriaceae, Erwiniaceae fam. nov., Pectobacteriaceae fam. nov., Yersiniaceae fam. nov., Hafniaceae fam. nov., Morganellaceae fam. nov., and Budviciaceae fam. nov. Int J Syst Evol Microbiol 66:5575–5599. https://doi.org/10.1099/ijsem.0.001485.
30. Strauch E, Kaspar H, Schaudinn C, Damasko C, Konietzny A, Dersch P, Skurnik M, Appel B. 2003. Analysis of enterocoliticin, a phage tail-like bacteriocin. Adv Exp Med Biol 529:249–251. https://doi.org/10.1007/0-306-48416-1_48.
31. Liu J, Chen P, Zheng C, Huang Y-P. 2013. Characterization of maltocin P28, a novel phage tail-like bacteriocin from Stenotrophomonas maltophilia. Appl Environ Microbiol 79:5593–5600. https://doi.org/10.1128/AEM.01648-13.

32. Jabrane A, Sabri A, Compere P, Jacques P, Vandenberghe I, Van Beeumen J, Thonart P. 2002. Characterization of serracin P, a phage-tail-like bacteriocin, and its activity against Erwinia amylovora, the fire blight pathogen. Appl Environ Microbiol 68:5704–5710. https://doi.org/10.1128/AEM.68.11.5704-5710.2002.
33. Delgado MA, Vincent PA, Farias RN, Salomon RA. 2005. YojI of Escherichia coli functions as a microcin J25 efflux pump. J Bacteriol 187:3465–3470. https://doi.org/10.1128/JB.187.10.3465-3470.2005.
34. Takeda Y, Kageyama M. 1975. Subunit arrangement in the extended sheath of pyocin R. J Biochem 77:679–684. https://doi.org/10.1093/oxfordjournals.jbchem.a130770.
35. Zinke M, Schröder GF, Lange A. 2022. Major tail proteins of bacteriophages of the order Caudovirales. J Biol Chem 298:101472. https://doi.org/10.1016/j.jbc.2021.101472.
36. Hu B, Margolin W, Molineux IJ, Liu J. 2015. Structural remodeling of bacteriophage T4 and host membranes during infection initiation. Proc Natl Acad Sci U S A 112:E4919–E4928. https://doi.org/10.1073/pnas.1501064112.
37. Feucht A, Schmid A, Benz R, Schwarz H, Heller KJ. 1990. Pore formation associated with the tail-tip protein pb2 of bacteriophage T5. J Biol Chem 265:18561–18567. https://doi.org/10.1016/S0021-9258(17)44788-0.
38. Zakharian E, Reusch RN. 2005. Kinetics of folding of Escherichia coli OmpA from narrow to large pore conformation in a planar bilayer. Biochemistry 44:6701–6707. https://doi.org/10.1021/bi047278e.
39. Gray M, Szabo G, Otero AS, Gray L, Hewlett E. 1998. Distinct mechanisms for K+ efflux, intoxication, and hemolysis by Bordetella pertussis AC toxin. J Biol Chem 273:18260–18267. https://doi.org/10.1074/jbc.273.29.18260.
40. Maier E, Reinhard N, Benz R, Frey J. 1996. Channel-forming activity and channel size of the RTX toxins ApxI, ApxII, and ApxIII of Actinobacillus pleuropneumoniae. Infect Immun 64:4415–4423. https://doi.org/10.1128/iai.64.11.4415-4423.1996.
41. Benz R, Maier E, Ladant D, Ullmann A, Sebo P. 1994. Adenylate cyclase toxin (CyaA) of Bordetella pertussis. Evidence for the formation of small ion-permeable channels and comparison with HlyA of Escherichia coli. J Biol Chem 269:27231–27239. https://doi.org/10.1016/S0021-9258(18)46973-6.
42. Bárcena-Uribarri I, Benz R, Winterhalter M, Zakharian E, Balashova N. 2015. Pore forming activity of the potent RTX-toxin produced by pediatric pathogen Kingella kingae: characterization and comparison to other RTX-family members. Biochim Biophys Acta 1848:1536–1544. https://doi.org/10.1016/j.bbamem.2015.03.036.
43. Wang SY, Zhao ZY, Haque F, Guo PX. 2018. Engineering of protein nanopores for sequencing, chemical or protein sensing and disease diagnosis. Curr Opin Biotechnol 51:80–89. https://doi.org/10.1016/j.copbio.2017.11.006.
44. Heron AJ, Thompson JR, Mason AE, Wallace MI. 2007. Direct detection of membrane channels from gels using water-in-oil droplet bilayers. J Am Chem Soc 129:16042–16047. https://doi.org/10.1021/ja075715h.
45. Schwartz JL, Lu YJ, Söhnlein P, Brousseau R, Laprade R, Masson L, Adang MJ. 1997. Ion channels formed in planar lipid bilayers by Bacillus thuringiensis toxins in the presence of Manduca sexta midgut receptors. FEBS Lett 412:270–276. https://doi.org/10.1016/s0014-5793(97)00801-6.
46. Song LZ, Hobaugh MR, Shustak C, Cheley S, Bayley H, Gouaux JE. 1996. Structure of staphylococcal alpha-hemolysin, a heptameric transmembrane pore. Science 274:1859–1866. https://doi.org/10.1126/science.274.5294.1859.
47. Krasilnikov OV, Sabirov RZ, Ternovsky VI, Merzliak PG, Muratkhodjaev JN. 1992. A simple method for the determination of the pore radius of ion channels in planar lipid bilayer membranes. FEMS Microbiol Immunol 5:93–100. https://doi.org/10.1111/j.1574-6968.1992.tb05891.x.
48. Merzlyak PG, Yuldasheva LN, Rodrigues CG, Carneiro CMM, Krasilnikov OV, Bezrukov SM. 1999. Polymeric nonelectrolytes to probe pore geometry: application to the alpha-toxin transmembrane channel. Biophys J 77:3023–3033. https://doi.org/10.1016/S0006-3495(99)77133-X.
49. Rubinson KA, Krueger S. 2009. Poly(ethylene glycol)s 2000–8000 in water may be planar: a small-angle neutron scattering (SANS) structure study. Polymer (Guildf) 50:4852–4858. https://doi.org/10.1016/j.polymer.2009.08.023.
50. Oelmeier SA, Dismer F, Hubbuch J. 2012. Molecular dynamics simulations on aqueous two-phase systems-single PEG-molecules in solution. BMC Biophys 5:14. https://doi.org/10.1186/2046-1682-5-14.
51. Jessberger N, Dietrich R, Schauer K, Schwemmer S, Martlbauer E, Benz R. 2020. Characteristics of the protein complexes and pores formed by Bacillus cereus hemolysin BL. Toxins (Basel) 12:672. https://doi.org/10.3390/toxins12110672.
52. Nováček J, Šiborová M, Benešík M, Pantůček R, Doškař J, Plevka P. 2016. Structure and genome release of Twort-like Myoviridae phage with a double-layered baseplate. Proc Natl Acad Sci U S A 113:9351–9356. https://doi.org/10.1073/pnas.1605883113.
53. Zinke M, Sachowsky KAA, Oster C, Zinn-Justin S, Ravelli R, Schroder GF, Habeck M, Lange A. 2020. Architecture of the flexible tail tube of bacteriophage SPP1. Nat Commun 11. https://doi.org/10.1038/s41467-020-19611-1.
54. Robertson JWF, Rodrigues CG, Stanford VM, Rubinson KA, Krasilnikov OV, Kasianowicz JJ. 2007. Single-molecule mass spectrometry in solution using a solitary nanopore. Proc Natl Acad Sci U S A 104:8207–8211. https://doi.org/10.1073/pnas.0611085104.
55. Derrington IM, Craig JM, Stava E, Laszlo AH, Ross BC, Brinkerhoff H, Nova IC, Doering K, Tickman BI, Ronaghi M, Mandell JG, Gunderson KL, Gundlach JH. 2015. Subangstrom single-molecule measurements of motor proteins using a nanopore. Nat Biotechnol 33:1073–1075. https://doi.org/10.1038/nbt.3357.
56. Derrington IM, Butler TZ, Collins MD, Manrao E, Pavlenok M, Niederweis M, Gundlach JH. 2010. Nanopore DNA sequencing with MspA. Proc Natl Acad Sci U S A 107:16060–16065. https://doi.org/10.1073/pnas.1001831107.
57. Reiner JE, Kasianowicz JJ, Nablo BJ, Robertson JWF. 2010. Theory for polymer analysis using nanopore-based single-molecule mass spectrometry. Proc Natl Acad Sci U S A 107:12080–12085. https://doi.org/10.1073/pnas.1002194107.
58. Deamer D, Akeson M, Branton D. 2016. Three decades of nanopore sequencing. Nat Biotechnol 34:518–524. https://doi.org/10.1038/nbt.3423.
59. Kasianowicz JJ, Robertson JWF, Chan ER, Reiner JE, Stanford VM. 2008. Nanoscopic porous sensors. Annu Rev Anal Chem (Palo Alto Calif) 1:737–766. https://doi.org/10.1146/annurev.anchem.1.031207.112818.
60. Lee G, Chakraborty U, Gebhart D, Govoni GR, Zhou ZH, Scholl D. 2016. F-type bacteriocins of Listeria monocytogenes: a new class of phage tail-like structures reveals broad parallel coevolution between tailed bacteriophages and high-molecular-weight bacteriocins. J Bacteriol 198:2784–2793. https://doi.org/10.1128/JB.00489-16.
61. Johnson CL, Ridley H, Pengelly RJ, Salleh MZ, Lakey JH. 2013. The unstructured domain of colicin N kills Escherichia coli. Mol Microbiol 89:84–95. https://doi.org/10.1111/mmi.12260.
62. Nikoleli G-P, Siontorou CG, Nikolelis M-T, Bratakou S, Bendos DK. 2019. Recent lipid membrane-based biosensing platforms. Appl Sci 9:1745. https://doi.org/10.3390/app9091745.
63. Nicolai C, Sachs F. 2013. Solving ion channel kinetics with the QuB software. Biophys Rev Lett 08:191–211. https://doi.org/10.1142/S1793048013300053.
64. Látrová K, Havlová N, Večeřová R, Pinkas D, Bogdanová K, Kolář M, Fišer R, Konopásek I, Do Pham DD, Rejman D, Mikušová G. 2021. Outer membrane and phospholipid composition of the target membrane affect the antimicrobial potential of first- and second-generation lipophosphonoxins. Sci Rep 11:10446. https://doi.org/10.1038/s41598-021-89883-0.
65. Aguilella VM, Queralt-Martín M, Aguilella-Arzo M, Alcaraz A. 2011. Insights on the permeability of wide protein channels: measurement and interpretation of ion selectivity. Integr Biol (Camb) 3:159–172. https://doi.org/10.1039/c0ib00048e.
66. Goldman DE. 1943. Potential, impedance, and rectification in membranes. J Gen Physiol 27:37–60. https://doi.org/10.1085/jgp.27.1.37.